

Modeling of Imbalance in Differential Lines Targeted to SPICE Simulation

Flavia Grassi^{1, *}, Xinglong Wu², Yuehong Yang²,
Giordano Spadacini¹, and Sergio A. Pignari¹

Abstract—In this paper, a SPICE model representative for the mode conversion occurring in differential lines affected by imbalance either of the line cross-section and the terminal networks is developed. The model is based on the assumption of weak imbalance and allows approximate prediction of modal quantities, through separate modeling of the contributions due to line and termination imbalance by controlled sources with (possibly) frequency dependent gain. The proposed SPICE model is used to perform worst-case prediction of undesired modal voltages induced at line terminals by mode conversion.

1. INTRODUCTION

Transmission technologies based on differential signaling (e.g., Low-Voltage Differential Signaling [1]) are key-ingredients of high-speed data links assuring satisfactory performance in terms of electromagnetic compatibility (EMC) and signal integrity (SI). However, in order for differential signaling to achieve effectiveness, the physical layer, including wiring harnesses and terminal networks, should meet stringent requirements in terms of balancing. Indeed, undesired asymmetries affecting the wiring structure or the terminal networks may give rise to unexpected conversion of differential mode (DM) into common mode (CM), and vice versa [2–4], with detrimental effects in terms of: (a) near- and far-field radiated emissions (ideally null) [5–7]; (b) degradation of CM-rejection properties and consequent susceptibility to the electromagnetic fields generated by nearby devices (radiated susceptibility, RS), [6], and to ground-bounce noise (conducted susceptibility, CS), [8, 9]. Additionally, balancing plays a crucial role in crosstalk mitigation [10]. Hence the interest, also from the prescriptive viewpoint [11], in characterizing, both theoretically and experimentally [12, 13], the degree of imbalance of cables and interconnections for high-speed communications, so to trouble-shoot and possibly fix the ensuing EMC and SI problems.

In line with this need, the present work is aimed at theoretically investigating the mechanism of mode conversion occurring in differential lines affected by asymmetries both in the line cross-section (line imbalance [14, 15]) and in the terminal networks (termination imbalance, [6]), with the objective to provide worst-case prediction of the overall disturbance induced at the terminal networks. Unlike in previous works, where the above-mentioned contributions to differential line (DL) imbalance were separately treated, suitable assumptions (usually satisfied in practical cases) are here introduced to allow for both phenomena at the same time. Target of the analysis is the development of a circuit model easy to be implemented and simulated in SPICE. Indeed, the development of prediction tools aimed at EMC-oriented simulation of wiring harnesses [16–18] and digital interconnects [19, 20] in this specific simulation environment has recently gained increasing attention from the EMC and SI communities.

The proposed study, involving Multi-conductor Transmission Line (MTL) theory and modal analysis, is based on the assumption that the DL circuit is weakly unbalanced (assumption made

Received 23 January 2015, Accepted 16 March 2015, Scheduled 20 March 2015

* Corresponding author: Flavia Grassi (flavia.grassi@polimi.it).

¹ Dipartimento di Elettronica, Informazione e Bioingegneria, Politecnico di Milano, Milano, Italy. ² State Key Lab of Electrical Insulation and Power Equipment, Xi'an Jiaotong University, Xi'an, Shaanxi, China.

practically sound by the fact that imbalance is usually to be ascribed to tolerances and non-ideal behavior of components) [6]. By virtue of such an assumption: (a) the contributions due to line and termination imbalance (separately predicted) can be superimposed yielding the overall modal quantities at line terminals; and (b) conversion of the dominant mode (DM/CM) excited by the signal (or noise) source into CM/DM (secondary mode) is treated as a one-way effect, so that re-conversion (back-interaction [10]) of the secondary mode onto primary quantities may be ignored [6]. The resulting SPICE model enables direct prediction of modal quantities at line terminals by recourse to the use of standard two-conductor transmission line parts and controlled sources (possibly with frequency dependent gain) only. Additionally, since the unbalanced DL is essentially treated as a perturbation of the corresponding balanced structure (reference), the proposed model allows sensitivity analyses and worst-case prediction of modal voltages/currents at the cost of time efficient simulations.

The model is initially developed for a DL composed of two bare wires running above a metallic ground (homogeneous medium), since this choice allows outlining the strict correlation of undesired voltages and currents at the DL terminations with geometrical and electrical asymmetries affecting the DL and its terminal networks. However, the proposed modeling approach is general, and can be easily extended (as it will be shown in Section 7) to the practically relevant case of DLs involving coated wire-pairs above ground (inhomogeneous medium).

The paper is organized as follows. In Section 2, the DL under analysis is introduced and transformed in the modal domain. Modeling strategies and assumptions are detailed in Section 3. In Sections 4 and 5, equivalent circuits representative for mode conversion are derived and validated versus exact solution of MTL equations. SPICE modeling is addressed in Section 6, while Section 7 deals with model extension to the practically relevant case of coated wire-pairs. Conclusions are then drawn in Section 8.

2. STRUCTURE UNDER ANALYSIS

2.1. Description of the Differential Line

In order to investigate the mechanisms of mode conversion due to imbalance, the DL circuit in Figure 1 is considered. In this circuit, the line is driven from the left termination by a pair of voltage sources V_{S1} , V_{S2} , whose values can be conveniently selected in order to emulate DM or CM line excitation. The networks at the left ($X = L$) and right ($X = R$) terminations are modeled by T-lumped parameter circuits with series impedances Z_{1X} , Z_{2X} differing each other by $\Delta Z_X \in [0, Z_D/2]$, i.e.,

$$Z_{1X,2X} = Z_D/2 \pm \Delta Z_X, \quad X = L, R, \quad (1)$$

so to account for possible imbalance affecting line terminal networks. Additionally, the wiring structure (see Figure 2) is composed of two bare wires with equal radii r , separated by a distance d , and ideally running at the same height h above ground as in Figure 2(a). Possible imbalance affecting the line cross-section is accounted for by assuming that wire positioning may slightly differ from the reference cross-section [Figure 2(b)]. Hence, according to Figure 2(b) and in analogy to (1), the wire heights are

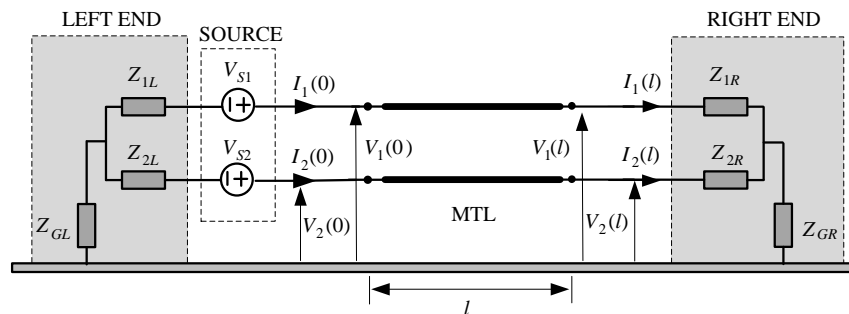


Figure 1. Principle drawing of the differential-line (DL) circuit under analysis.

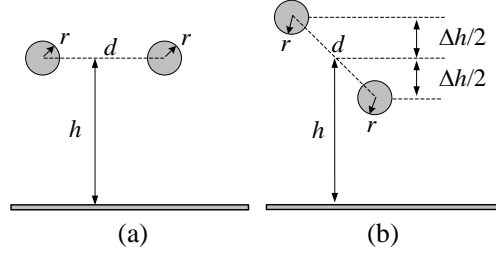


Figure 2. Line cross-section: (a) perfectly balanced (reference structure); (b) slightly unbalanced.

assumed to differ from the height of the cable axis by $\Delta h \in [0, d]$, i.e.,

$$h_{1,2} = h \pm \Delta h/2, \quad (2)$$

while wire separation, d , is kept constant.

2.2. MTL Modeling and Modal Analysis

Propagation and conversion of modal quantities in the above-described DL circuit are studied by combining multi-conductor transmission line (MTL) theory and modal analysis. Accordingly, the wiring structure is modeled as a uniform and lossless three-conductor MTL in free-space, with per unit length (p.u.l.) inductance and capacitance matrices

$$\mathbf{L} = \begin{bmatrix} \ell_1 & \ell_m \\ \ell_m & \ell_2 \end{bmatrix}, \quad \mathbf{C} = \begin{bmatrix} c_1 & c_m \\ c_m & c_2 \end{bmatrix} = \frac{1}{v_0^2} \mathbf{L}^{-1}, \quad (3)$$

where v_0 denotes the light velocity in free space. Additionally, CM and DM quantities are introduced starting from physical voltages and currents in Figure 1 by recourse to the transformation matrices in [15] as

$$\mathbf{V}_m = \begin{pmatrix} V_{cm} \\ V_{dm} \end{pmatrix} = \mathbf{T}_V^{-1} \cdot \begin{pmatrix} V_1 \\ V_2 \end{pmatrix}, \quad \mathbf{I}_m = \begin{pmatrix} I_{cm} \\ I_{dm} \end{pmatrix} = \mathbf{T}_I^{-1} \cdot \begin{pmatrix} I_1 \\ I_2 \end{pmatrix}. \quad (4)$$

$$\mathbf{T}_V = \begin{bmatrix} 1 & 0.5 \\ 1 & -0.5 \end{bmatrix}, \quad \mathbf{T}_I = \begin{bmatrix} 0.5 & 1 \\ 0.5 & -1 \end{bmatrix}. \quad (5)$$

Introduction of (4)–(5) allows rephrasing in the modal domain the MTL equations describing the wiring structure and its terminal sections. Hence, resorting to the chain-parameter representation, the relationships between modal voltages and currents at line terminals can be cast as:

$$\begin{pmatrix} \mathbf{V}_m(\ell) \\ \mathbf{I}_m(\ell) \end{pmatrix} = \begin{bmatrix} \cos(\beta\ell)\mathbf{1}_2 & -j \sin(\beta\ell)\mathbf{Z}_{C,m} \\ -j \sin(\beta\ell)\mathbf{Z}_{C,m}^{-1} & \cos(\beta\ell)\mathbf{1}_2 \end{bmatrix} \cdot \begin{pmatrix} \mathbf{V}_m(0) \\ \mathbf{I}_m(0) \end{pmatrix}, \quad (6)$$

where ℓ is the line length, $\beta = 2\pi f/v_0$ the CM and DM propagation constant (i.e., $\beta_{cm} = \beta_{dm} = \beta$, degenerate mode), $\mathbf{1}_2$ the 2×2 identity matrix, and $\mathbf{Z}_{C,m}$ the (2×2) characteristic impedance matrix in the modal domain. In particular, since in free-space the characteristic impedance matrix \mathbf{Z}_C is proportional to the p.u.l. length inductance matrix in (3) as $\mathbf{Z}_C = v_0 \mathbf{L}$, matrix $\mathbf{Z}_{C,m}$ in (6) takes the expression:

$$\mathbf{Z}_{C,m} = \mathbf{T}_V^{-1} \mathbf{Z}_C \mathbf{T}_I = \begin{bmatrix} Z_{cm} & \Delta Z_\ell \\ \Delta Z_\ell & Z_{dm} \end{bmatrix} = \frac{v_0}{2} \begin{bmatrix} \frac{\ell_1 + \ell_2}{2} + \ell_m & \ell_1 - \ell_2 \\ \ell_1 - \ell_2 & 2(\ell_1 + \ell_2 - 2\ell_m) \end{bmatrix}. \quad (7)$$

In a similar fashion, if the impedance matrices associated with the passive part of the terminal networks in Figure 1 are converted in the modal domain, the following general expression ($X = L, R$) is obtained

$$\mathbf{Z}_{X,m} = \begin{bmatrix} Z_{GX} + Z_D/4 & \Delta Z_X \\ \Delta Z_X & Z_D \end{bmatrix} = \begin{bmatrix} Z_{CM} & \Delta Z_X \\ \Delta Z_X & Z_{DM} \end{bmatrix}. \quad (8)$$

From the above matrices, the occurrence of mode conversion can be readily ascribed to the presence of the non-null out-diagonal entries ΔZ_ℓ , ΔZ_X . These parameters represent a measure of the different impedance seen by each of the two wires with respect to ground at the terminal sections (ΔZ_X) or at each position along the DL (ΔZ_ℓ). Accordingly, the former contribution (i.e., imbalance due to line terminations) is responsible for lumped mode conversion at the DL ends, whereas the latter (i.e., imbalance due to asymmetries in the line cross-section) gives rise to distributed mode conversion along the DL. Conversely, if the interconnection and its terminal networks were perfectly balanced, out-diagonal entries in (7)–(8) would be null, i.e., $\Delta Z_\ell = \Delta Z_X = 0$, and CM and DM quantities would propagate separately.

3. MODELING STRATEGY

Starting from the DL circuit in Figure 1, DM to CM and, vice versa, CM to DM conversions are separately analyzed by setting V_{S1} , V_{S2} to the values: (a) $V_{S1} = -V_{S2} = 1/2V_S$, and (b) $V_{S1} = V_{S2} = V_S$, respectively. Namely, according to (4), the former set leads to pure DM excitation (i.e., $V_{dm} = V_S$, $V_{cm} = 0$) and it is suitable to analyze DM-to-CM conversion. Conversely, the latter set leads to pure CM excitation (i.e., $V_{cm} = V_S$, $V_{dm} = 0$) and will be used to study the opposite conversion mechanism. Although this choice is here aimed at studying the two mechanisms separately, however this is in line with typical EMC troubleshooting strategies, which are based on the fact that in EMC problems is often possible to identify a dominant mode [6]. Additionally, the modeling approach here adopted is based on the observation that imbalance either due to terminal networks and due to asymmetries in the line cross-section arise from imperfection or tolerance in the manufacture process. Therefore, in practical cases, the overall imbalance is weak, with the consequences in terms of modeling that will be made clear in the following sub-sections.

3.1. Superposition Principle

As the first consequence of weak imbalance, the unbalanced DL can be interpreted as a perturbation of the corresponding balanced structure. This means that modal matrices in (7)–(8) can be re-written as:

$$\mathbf{Z}_{C,m} = \mathbf{Z}_{C,m}^{bal} + \begin{bmatrix} 0 & \Delta Z_\ell \\ \Delta Z_\ell & 0 \end{bmatrix}, \quad (9)$$

$$\mathbf{Z}_{X,m} = \mathbf{Z}_{X,m}^{bal} + \begin{bmatrix} 0 & \Delta Z_X \\ \Delta Z_X & 0 \end{bmatrix}, \quad (10)$$

where $\mathbf{Z}_{C,m}^{bal}$, $\mathbf{Z}_{X,m}^{bal}$ denote the characteristic impedance and termination impedance matrices, respectively, of the balanced structure. The equality in (10) can be readily proved by setting $\Delta Z_X = 0$ in (1). Conversely, a proof for (9) can be provided by exploiting the approximate analytical expressions for the p.u.l. parameters of a pair of bare wires running above ground in [10], and by comparing the results obtained for the balanced (a) and unbalanced (b) cross-sections in Figure 2. After some algebra (here omitted for brevity) and as long as $(2h)^2 \gg \Delta h^2$, d^2 , it is proved that the diagonal entries of $\mathbf{Z}_{C,m}$ are equal to the modal characteristic impedances of the balanced line in Figure 2(a), i.e.,

$$Z_{cm} = Z_{cm}^{bal} \cong 60 \ln \left(2h / \sqrt{r d} \right) \quad (11)$$

$$Z_{dm} = Z_{dm}^{bal} \cong 120 \ln(d/r), \quad (12)$$

and the imbalanced coefficient ΔZ_ℓ can be expressed as function of geometrical parameters as

$$\Delta Z_\ell = v_0 \frac{\ell_1 - \ell_2}{2} \cong 30 \ln \left(1 + \frac{\Delta h}{h} \right) \cong 30 \frac{\Delta h}{h}. \quad (13)$$

In a similar way, also $\mathbf{Z}_{C,m}^{-1}$ in (6) can be written as:

$$\mathbf{Z}_{C,m}^{-1} = \mathbf{T}_I^{-1}(v_0 \mathbf{C}) \mathbf{T}_V = \begin{bmatrix} Z_{cm}^{-1} & v_0 \frac{c_1 - c_2}{2} \\ v_0 \frac{c_1 - c_2}{2} & Z_{dm}^{-1} \end{bmatrix} = \left(\mathbf{Z}_{C,m}^{bal} \right)^{-1} + \frac{1}{Z_{cm} Z_{dm}} \begin{bmatrix} 0 & -\Delta Z_\ell \\ -\Delta Z_\ell & 0 \end{bmatrix} \quad (14)$$

on condition that $\Delta Z_\ell^2 / (Z_{cm} Z_{dm}) \ll 1$.

Writing modal matrices $\mathbf{Z}_{C,m}$, $\mathbf{Z}_{C,m}^{-1}$ and $\mathbf{Z}_{X,m}$ as in (9)–(10), (14) enables to study the effects due to line and termination imbalance separately, and to subsequently superimpose the two effects (by the superposition principle) to predict the overall modal voltages and currents at line terminals.

3.2. Negligible Back-Interaction on the Dominant Mode

The second consequence of weak imbalance is that the back-interaction on the dominant mode of currents and voltages excited by mode conversion in the secondary mode is negligible. For instance, if the DL is driven by a DM source (i.e., if $V_{S1} = -V_{S2} = 1/2V_S$), the modal matrices in (9)–(10), (14) can be further approximated as:

$$\mathbf{Z}_{C,m} \cong \mathbf{Z}_{C,m}^{bal} + \begin{bmatrix} 0 & \Delta Z_\ell \\ 0 & 0 \end{bmatrix}, \quad \mathbf{Z}_{C,m}^{-1} \cong \left(\mathbf{Z}_{C,m}^{bal}\right)^{-1} + \begin{bmatrix} 0 & -\frac{\Delta Z_\ell}{Z_{cm} Z_{dm}} \\ 0 & 0 \end{bmatrix}, \quad (15)$$

$$\mathbf{Z}_{X,m} \cong \mathbf{Z}_{X,m}^{bal} + \begin{bmatrix} 0 & \Delta Z_X \\ 0 & 0 \end{bmatrix}, \quad (16)$$

and the system of equations for the DM (dominant mode) can be cast and solved as the first step as

$$\begin{pmatrix} V_{dm}(\ell) \\ I_{dm}(\ell) \end{pmatrix} \cong \begin{bmatrix} \cos(\beta\ell) & -j \sin(\beta\ell) Z_{dm} \\ -j \sin(\beta\ell) Z_{dm}^{-1} & \cos(\beta\ell) \end{bmatrix} \cdot \begin{pmatrix} V_{dm}(0) \\ I_{dm}(0) \end{pmatrix}, \quad (17)$$

$$V_{dm}(0) \cong V_S - Z_D I_{dm}(0), \quad V_{dm}(\ell) \cong Z_D I_{dm}(\ell), \quad (18)$$

where all contributions due to the CM (secondary mode) are disregarded. Similar results, omitted for brevity, are obtained for CM quantities when the DL is driven by the CM source $V_{S1} = V_{S2} = V_S$. Therefore, under the assumption of weak imbalance, voltages and currents of the dominant mode can be computed as the wiring structure and its terminal networks were perfectly balanced, by solution of the equivalent modal circuits in Figure 3.

Accuracy of the prediction obtained by the approximate modal circuits in Figure 3 can be proven by comparison versus exact solution of MTL equations. As a specific example, a 1 m-long wiring structure composed of two bare wires with radius $r = 0.5$ mm, wire distance $d = 2.5$ mm, nominal height $h = 50$ mm, and fed by a pure DM source $V_{S1} = -V_{S2} = 0.5$ V is considered. The plots in Figure 4 represent DM voltages at the right DL-end for different degrees of line and termination imbalance and for ground impedances $Z_{GL} = Z_{GR} = 0 \Omega$ (worst-case condition for termination imbalance [6]). The comparison clearly shows that DM voltages are not influenced by possible imbalance affecting either the line cross-section or the terminal networks even for uncertainties on the values of the series impedances in (1) on the order of 40% (in this case, the maximum differences observed in Figure 4 are on the order of 0.3 dB).

4. DM-TO-CM CONVERSION

Under the assumption of weak unbalance, DM-to-CM conversion is investigated in this Section by preliminary solving the DM circuit in Figure 3(a), and by applying the superposition principle to

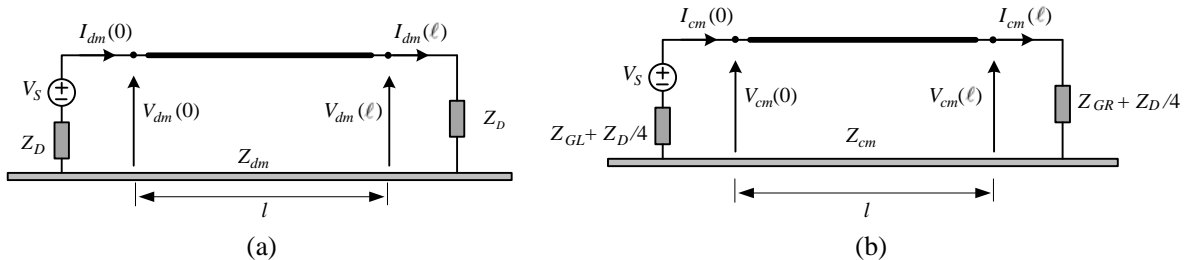


Figure 3. Approximate (a) DM and (b) CM circuits obtained under the assumption of weak unbalance for (a) DM and (b) CM excitation of the DL circuit in Figure 1.

combine the contributions due to the imbalance affecting the line cross-section and the terminal networks.

4.1. Contribution Due to Termination Imbalance

To evidence imbalance due to line terminations, the line cross-section is assumed to be perfectly balanced and the corresponding unbalance coefficient ΔZ_ℓ in (15) is set equal to zero. Accordingly, (6) and (15)–(16) lead to the following system of equations for the prediction of CM voltages and currents at line terminals:

$$\begin{pmatrix} V_{cm}(\ell) \\ I_{cm}(\ell) \end{pmatrix} \cong \begin{bmatrix} \cos(\beta\ell) & -j \sin(\beta\ell) Z_{cm} \\ -j \sin(\beta\ell) Z_{cm}^{-1} & \cos(\beta\ell) \end{bmatrix} \cdot \begin{pmatrix} V_{cm}(0) \\ I_{cm}(0) \end{pmatrix}, \quad (19)$$

$$V_{cm}(0) + Z_{CM} I_{cm}(0) = -\Delta Z_L I_{dm}(0) = V_{TL} \quad (20)$$

$$V_{cm}(\ell) - Z_{CM} I_{cm}(\ell) = \Delta Z_R I_{dm}(\ell) = V_{TR}. \quad (21)$$

This system of equations allows the circuit interpretation in Figure 5(a), which shows that the effect due to termination imbalance can be modelled into the CM circuit by two voltage sources connected at line terminals and proportional to the DM currents and to the degree of imbalance of each terminal networks [6].

4.2. Contribution Due to Line Imbalance

In a similar fashion, the contribution due to line imbalance can be analyzed starting from the equations in (6), (15)–(16) by assuming the terminal networks perfectly balanced (i.e., $\Delta Z_L = \Delta Z_R = 0$). Hence, CM voltages and currents at line ends can be predicted by the following system of equations:

$$\begin{pmatrix} V_{cm}(\ell) \\ I_{cm}(\ell) \end{pmatrix} \cong \begin{bmatrix} \cos(\beta\ell) & -j \sin(\beta\ell) Z_{cm} \\ -j \sin(\beta\ell) Z_{cm}^{-1} & \cos(\beta\ell) \end{bmatrix} \cdot \begin{pmatrix} V_{cm}(0) \\ I_{cm}(0) \end{pmatrix} + \begin{pmatrix} V_\Delta \\ I_\Delta \end{pmatrix} \quad (22)$$

$$V_{cm}(0) = -Z_{CM} I_{cm}(0), \quad V_{cm}(\ell) = Z_{CM} I_{cm}(\ell), \quad (23)$$

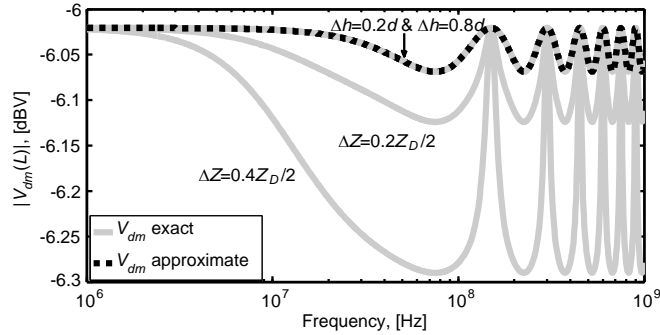


Figure 4. DM voltages at the right DL end ($Z_D = 0.9Z_{dm}$, $Z_{GL(R)} = 0\Omega$). Solid grey curves: exact solution of MTL equations. Dashed-black curve: DM circuit in Figure 3(a).

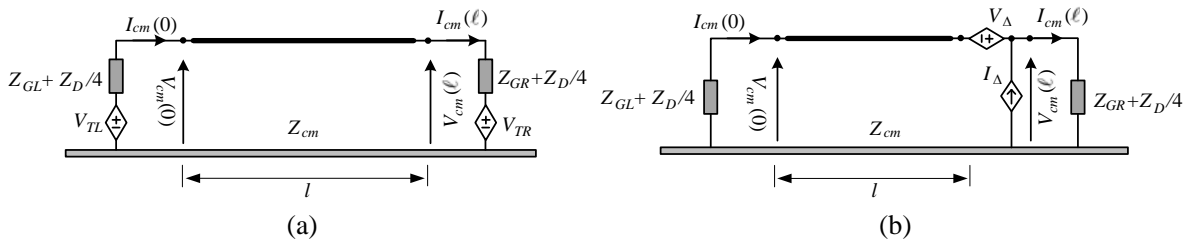


Figure 5. CM circuits accounting for DM-to-CM conversion due to (a) line and (b) termination imbalance.

where:

$$V_{\Delta} = -j \sin(\beta\ell) \Delta Z_{\ell} I_{dm}(0), \quad (24)$$

$$I_{\Delta} = j \sin(\beta\ell) \Delta Z_{\ell} (Z_{cm} Z_{dm})^{-1} V_{dm}(0). \quad (25)$$

A circuit interpretation of (22)–(25) is shown in Figure 5(b), where effects due to imbalance of the line cross-section are included into the CM circuit by the voltage and current sources V_{Δ} , I_{Δ} . Likewise those in (20)–(21), these sources are proportional to the imbalance coefficient ΔZ_{ℓ} and to DM currents and voltages at the terminations of the DM circuit in Figure 3(a). However, they are actually representative of a distributed instead of a lumped mechanism of mode conversion, and can be lumped at one termination (here the right one) only as long as prediction of voltages and currents at line terminals is the target.

As a matter of fact, their amplitudes depend on the line length and operating frequency through the sinus term. More precisely, as long as the line length is sufficiently smaller than the wavelength $\lambda = v_0/f$, it can be shown that V_{Δ} , I_{Δ} are proportional to the ratio ℓ/λ , and become null for frequency approaching zero. Conversely, the sources in (20)–(21) are independent of frequency apart from the frequency dependence of the involved DM currents. Nevertheless, in this respect it's worth noting that in practical cases ΔZ_L , ΔZ_R are inherently frequency dependent, since balance performance of terminal networks generally degrade at increasing frequency. For instance, frequency performance of typical center-tap RF transformers (baluns) can be considered [8].

4.3. Validation and Comparative Analysis

In this subsection, model accuracy is preliminary validated versus exact solution of MTL equations. Specific examples are shown in Figure 6 and Figure 7.

Regarding termination imbalance, the plots in Figure 6 show that minimum values of the ground impedances (for simulation: $Z_{GL} = Z_{GR} = Z_G = 0, 1 \text{ k}\Omega$) lead to worst-case conditions both in terms of (a) accuracy of the prediction model, and (b) maximum CM voltages induced at line terminals. However, even in this condition a remarkable accuracy is achieved (discrepancies on the order of few dBs are observed at low frequency only) even for relatively large imbalance coefficients (on the order of 40% of the nominal value, i.e., $Z_D/2$). Additionally, comparison of the plots in Figure 6(a) and Figure 6(b) shows that, assigned a specific value to the coefficients $|\Delta Z_L| = \Delta Z_R$, the frequency response of the involved CM voltages may deeply differ at low frequency depending on the specific combination of the two voltage sources in Figure 5(a). In the specific test case $\Delta Z_L = \Delta Z_R$, [Figure 6(a)] the two contributions perfectly balance each other at low frequency, so that CM voltages increase by a +20 dB/dec frequency slope. Conversely, if the two coefficients are equal but opposite in sign (i.e., $\Delta Z_L = -\Delta Z_R$) as in Figure 6(b), the transfer function between the DM source V_S and the CM voltages at line terminals is constant at low frequency with amplitude $|\Delta Z_L|/Z_D$.

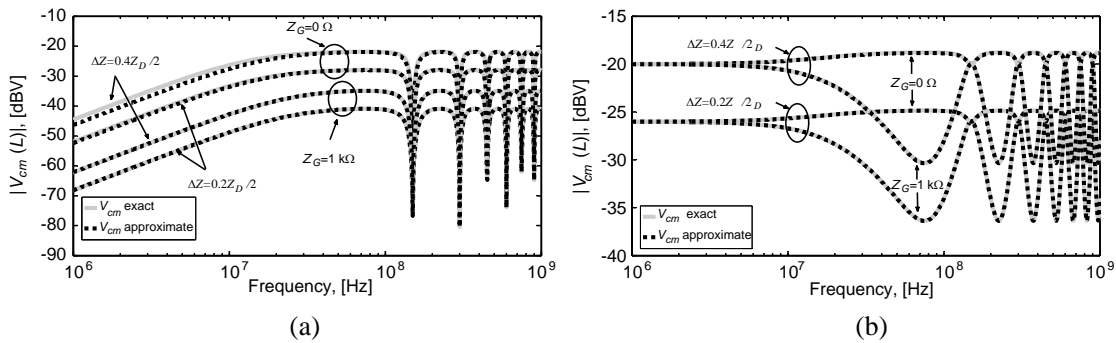


Figure 6. CM voltages due to termination imbalance: proposed model (dotted curves) vs exact MTL solution (grey-solid curves). Influence of the ground impedance (i.e., $Z_G = 0 \Omega, 1 \text{ k}\Omega$) for (a) $\Delta Z = \Delta Z_L = \Delta Z_R$, (b) $\Delta Z = \Delta Z_L = -\Delta Z_R$.

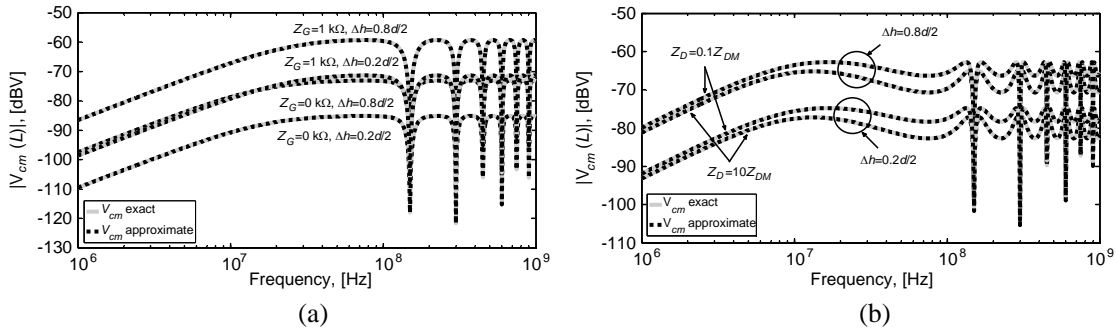


Figure 7. CM voltages due to line imbalance: Proposed model (dotted curves) vs exact MTL solution (grey-solid curves). Influence of (a) ground impedance $Z_G = 0\Omega$, $1\text{ k}\Omega$, and (b) mismatching (i.e., $Z_D \neq Z_{dm}$) of the DM circuit ($Z_G = 1\text{ k}\Omega$).

Concerning line imbalance, the plots in Figure 7 investigate the influence on CM voltages of the ground impedances [Figure 7(a)] and of possible mismatching at the terminations of the DM circuit [Figure 7(b)]. By the light of these results, the following differences with respect to termination imbalance can be stated. First, at low frequency CM voltages due to line imbalance always increase with $+20\text{ dB/dec}$ frequency slope, due to the distributed nature of mode conversion. Second, maximum CM voltages are induced at line terminals for large (instead of minimum) values of the ground impedances Z_G [in Figure 7(a) for $Z_G = Z_{GL} = Z_{GR} = 1\text{ k}\Omega$]. Third, since amplitudes and relative signs of the current and voltage sources V_Δ , I_Δ descend from geometrical properties of the line cross-section, it can be easily proven that contributions due to these sources always sum at the left termination (i.e., close to the signal source), and subtract at the right-end. Therefore, CM voltages at the left termination are larger or, at worst, equal to those at the right termination. As far as model accuracy is concerned, since Δh is very small with respect to h (i.e., $h \gg d$), the weak imbalance assumption is always satisfied for $\Delta h \in [0, d]$. Namely, the plots in Figure 7 show that even for large degrees of imbalance [upper curves in Figure 7(a)] and strong mismatching of the DM circuit [Figure 7(b)] the differences between exact (grey-solid curves) and approximate (black-dotted curves) predictions is negligible for whatever values of Z_{GL} , Z_{GR} .

4.4. Superposition of the Two Contributions

As long as the weak-imbalance assumption is satisfied, effects due to termination and line imbalance can be simultaneously accounted for by superimposing the proposed approximate models. This leads to the equivalent CM circuit in Figure 8, whose sources still involve the DM currents and voltages in Figure 3(a) through (20)–(21) and (24)–(25).

Specific examples of results are shown in Figure 9, where the overall CM voltage at the left termination is compared with the contributions due to line and termination imbalance. These plots were obtained for ground impedances equal to $Z_{GL(R)} = 1\text{ k}\Omega$ (condition leading to maximum contribution due to line imbalance and minimum contribution due to termination imbalance), and by assuming: $\Delta h = 0.4d$, $\Delta Z_L = \Delta Z_R = 0.05Z_D/2$. More precisely, the plots in Figure 9(a) were evaluated for

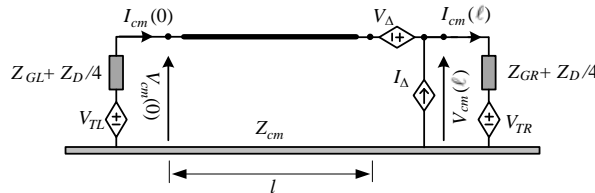


Figure 8. Equivalent CM circuit accounting for DM-to-CM conversion due to line and termination imbalance.

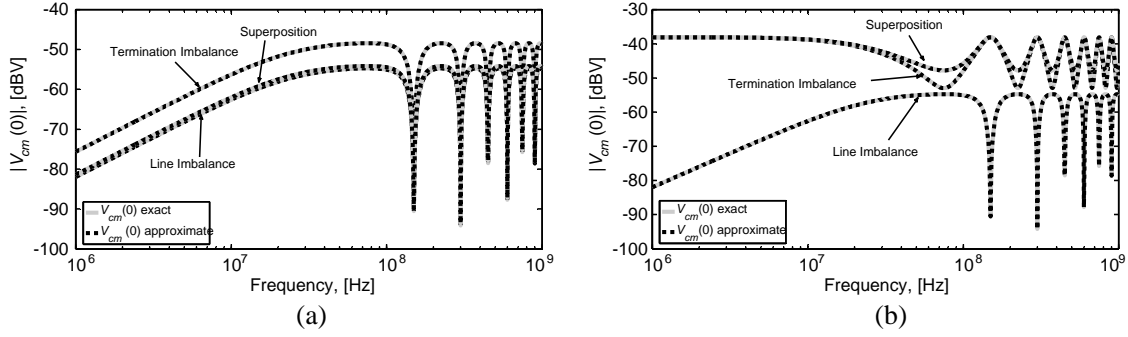


Figure 9. CM voltages obtained by superposition of the contributions due to line and termination imbalance ($Z_G = 1 \text{ k}\Omega$): (a) $\Delta Z_L = \Delta Z_R$; and (b) $\Delta Z_L = -\Delta Z_R$.

$\Delta Z_L = \Delta Z_R$, those in Figure 9(b) for $\Delta Z_L = -\Delta Z_R$. Solid-grey curves were obtained by exact solution of MTL equations, whereas dotted-black curves were predicted by the approximate model in Figure 8.

Besides proving model accuracy, these results show that — given specific degrees of imbalance — the two contributions may add or subtract each other, depending on the combination of signs of the involved imbalance coefficients. As a rule of thumb, for positive values of ΔZ_ℓ , the two contributions subtract each other if $\Delta Z_L, \Delta Z_R$ have the same sign [Figure 9(a)]. Conversely, if $\Delta Z_L, \Delta Z_R$ are opposite in sign (and $\Delta Z_\ell > 0$), the two contributions add each other and lead to the largest CM voltages.

5. CM-TO-DM CONVERSION

The proposed model can be successfully extended to analyze the opposite mechanism of conversion from CM (excited by the CM source $V_{S1} = V_{S2} = V_S$) to DM. Indeed, as long as the weak imbalance assumption is satisfied, CM voltages and currents at line terminals can be predicted as the first step by the CM equivalent circuit in Figure 3(b), and subsequently exploited as source terms, i.e.,

$$V'_\Delta = -j \sin(\beta\ell) \Delta Z_\ell I_{cm}(0), \quad (26)$$

$$I'_\Delta = j \sin(\beta\ell) \Delta Z_\ell (Z_{cm} Z_{dm})^{-1} V_{cm}(0), \quad (27)$$

$$V'_{TL} = -\Delta Z_L I_{cm}(0), \quad V'_{TR} = -\Delta Z_R I_{cm}(\ell) \quad (28)$$

in the equivalent DM circuit in Figure 10.

Simulation results, here omitted for the sake of brevity, proved the accuracy of such an approximate model even for relatively large degrees of imbalance affecting the wiring structure and its terminal loads. The most significant difference with respect to DM-to-CM conversion is concerned with the role played by the ground impedances Z_{GL}, Z_{GR} . Namely, for CM-to-DM conversion small values of Z_{GL}, Z_{GR} lead to maximum DM voltages due to line imbalance, while in the same condition, minimum CM voltages were obtained for DM-to-CM conversion. In particular, in the specific test case $Z_{GL} = Z_{GR} = 0$, DM voltages due to CM-to-DM conversion are four times larger (12 dB shift) than the corresponding CM voltages due to DM-to-CM conversion, due to the fact that the terminal impedances of the DM circuit in Figure 10 are four times larger than those of the equivalent CM circuit in Figure 8. Conversely, no significant differences with respect to DM-to-CM conversion are worth noting as far as (a) imbalance due to terminal loads, and (b) superposition of the two contributions are concerned.

6. SPICE MODELING

For SPICE implementation, a 1 m long DL characterized by the geometrical parameters in Subsection 3.2 and imbalance coefficients $\Delta h = d/2, \Delta Z_L = \Delta Z_R = 0.05 Z_D/2$ is considered. For such a DL, the SPICE schematic representative for DM into CM conversion is shown in Figure 11(a). In this model, three (instead of two) two-conductor TLs have been implemented (either by T or TLOSSY parts [21]), in

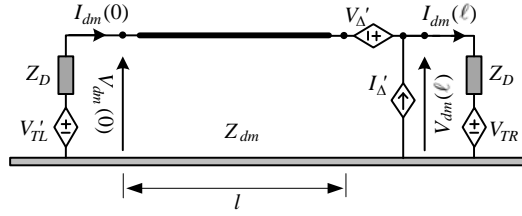


Figure 10. DM circuit accounting for CM-to-DM conversion due to line and termination imbalance.

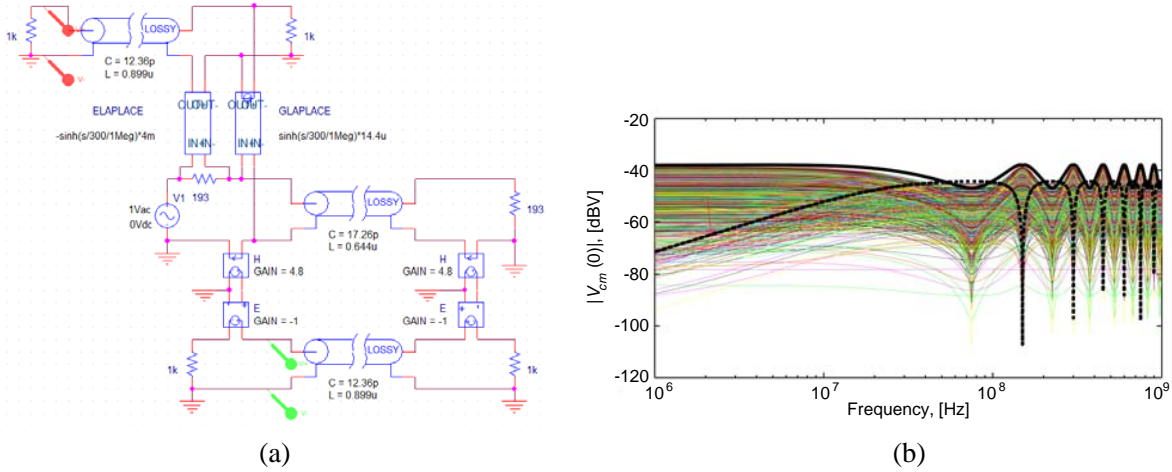


Figure 11. Implementation in SPICE: (a) schematic of the unbalanced DL excited by a DM source. (b) SPICE predictions (black curves) vs 1000 repeated simulations obtained by exact solution of MTL equations (left TL end).

order to allow separate evaluation of the two contributions to the overall CM voltages. Indeed, the TL in the middle represents the DM circuit (dominant mode), with characteristic impedance $Z_{dm} = 193 \Omega$, and, without loss of generality, matched terminations $Z_D = Z_{dm}$. The upper and lowest TMs are CM circuits, with characteristic impedance $Z_{cm} = 269 \Omega$ and terminal impedances $Z_{GL(R)} + Z_D/4 \approx 1 \text{ k}\Omega$. Particularly, the lowest CM circuit is used to predict the contribution due to termination imbalance. Accordingly, this circuit is fed at both terminations by current-controlled voltage sources with constant gain, i.e., $\Delta Z_L = \Delta Z_R = 4.8 \Omega$. Note that the additional voltage-controlled voltage sources (with unitary gains) are included to avoid crossed connections.

Conversely, implementation of the frequency-dependent sources accounting for line imbalance involves the ABM (Analog Behavioral Model) parts `ELAPLACE` and `GLAPLACE` [21]. These parts are voltage-controlled voltage (`ELAPLACE`) and current (`GLAPLACE`) sources, whose frequency-dependent gains are assigned in terms of Laplace transform. For the specific test case under analysis, the current source I_Δ in (25) is implemented by a `GLAPLACE` part with trans-admittance [according to (25)]

$$Y_\Delta(s) = \frac{I_\Delta}{V_{dm}(0)} \cong 14.4 \sinh(s T_D) \mu\Omega^{-1}, \quad (29)$$

where $T_D = \ell/v_0 = 10/3 \text{ ns}$, and controlled by the DM voltage at the left termination of the DM TL. Conversely, since ABM current-controlled sources are not available in SPICE, the voltage source V_Δ in (24) is implemented by an `ELAPLACE` part controlled — instead of by the DM current $I_{dm}(0)$ — by the voltage drop across the series impedance Z_D at the left DL end. According to this implementation, and in line with (24), the dimensionless gain of the involved `ELAPLACE` part takes the expression:

$$K_\Delta(s) = \frac{V_\Delta}{Z_D I_{dm}(0)} \cong -4 \cdot 10^{-3} \sinh(s T_D). \quad (30)$$

6.1. Worst-Case Analysis

Based on previous analysis, the SPICE schematic in Figure 11(a) can be conveniently exploited to predict worst-case CM voltages at DL terminations due to specific degrees of imbalance affecting the line cross-section and the DL terminal networks.

As an explicative example, let's assume that the imbalance coefficients may randomly vary (uniform distribution) within the intervals: $-d/2 \leq \Delta h \leq d/2$, and $-0.05Z_D/2 \leq \Delta Z_L, \Delta Z_R \leq 0.05Z_D/2$. Predictions for the CM voltages at the left termination obtained by 1000 repeated simulations based on exact solution of MTL equations are plotted (colored curves) in Figure 11(b). In spite of the wide spread of results, upper bounds to these curves can be readily obtained by running the SPICE schematic twice, and by summing (for each simulation) the magnitude of the contributions due to line and termination imbalance. In the former simulation, the unitary gains of the voltage-controlled voltage sources have the same sign as in Figure 11(a), in the latter, they have opposite signs. The obtained results are plotted in Figure 11(b) by dashed- and solid-black curves, respectively, that effectively upper-bound the colored curves in the considered frequency range.

7. INHOMOGENEOUS MEDIA

In this section, the weak-imbalance assumption and the superposition principle are exploited to extend the prediction model and associated SPICE schematic to the practically relevant case of DLs in inhomogeneous media. To this end, a dielectric coating with relative dielectric permittivity $\epsilon_r \neq 1$ is assumed to surround the two wires in the cable cross-section in Figure 2, and DM-to-CM conversion is investigated by driving the DL by a pure DM source $V_{S1} = -V_{S2} = 1/2V_S$ connected at the left terminal section (see Figure 1). The main steps of the derivation will be briefly reviewed, with the objective to outline analogies and differences with respect to the homogeneous case.

7.1. Model Extension

In the presence of inhomogeneous media, the line p.u.l. inductance and capacitance matrices take the same expressions in (3), with the difference that the p.u.l. capacitance matrix cannot be obtained any longer from the p.u.l. inductance matrix by the relationship $\mathbf{C} = v_0^{-2} \cdot \mathbf{L}^{-1}$, but requires numerical evaluation. Particularly, in the modal domain defined by the transformation matrices in (5), these p.u.l. matrices can still be written as a perturbation of those associated with the corresponding balanced structure as

$$\mathbf{L}_m = \mathbf{T}_V^{-1} \cdot \mathbf{L} \cdot \mathbf{T}_I \cong \mathbf{L}_m^{bal} + \begin{bmatrix} 0 & \Delta L \\ \Delta L & 0 \end{bmatrix}; \quad \mathbf{L}_m^{bal} = \begin{bmatrix} \ell_{cm} & 0 \\ 0 & \ell_{dm} \end{bmatrix} \quad (31)$$

$$\mathbf{C}_m = \mathbf{T}_I^{-1} \cdot \mathbf{C} \cdot \mathbf{T}_V \cong \mathbf{C}_m^{bal} + \begin{bmatrix} 0 & \Delta C \\ \Delta C & 0 \end{bmatrix}; \quad \mathbf{C}_m^{bal} = \begin{bmatrix} c_{cm} & 0 \\ 0 & c_{dm} \end{bmatrix} \quad (32)$$

where ℓ_{cm} , c_{cm} and ℓ_{dm} , c_{dm} denote the CM and DM p.u.l. inductance and capacitance associated with the balanced structure, whereas inductive and capacitive coefficients $\Delta L = (\ell_1 - \ell_2)/2$ and $\Delta C = (c_1 - c_2)/2$ account for the effects due to line imbalance. In line with (14), as long as these imbalance coefficients satisfy the inequalities $\Delta L^2 \ll \ell_{cm}\ell_{dm}$, $\Delta C^2 \ll c_{cm}c_{dm}$, the back-interaction of the CM on the DM can be neglected, and the p.u.l. modal matrices in (31)–(32) can be further simplified to

$$\mathbf{L}_m \cong \mathbf{L}_m^{bal} + \begin{bmatrix} 0 & \Delta L \\ 0 & 0 \end{bmatrix}; \quad \mathbf{C}_m \cong \mathbf{C}_m^{bal} + \begin{bmatrix} 0 & \Delta C \\ 0 & 0 \end{bmatrix}. \quad (33)$$

By virtue of (33) and in analogy to the homogeneous case, the DM circuit can be preliminary solved assuming the wiring structure to be perfectly balanced. Notice that the only difference with respect to the homogeneous case is related to the DM characteristic impedance and propagation velocity, here given by $Z_{dm} = \sqrt{\ell_{dm}/c_{dm}}$ and $v_{dm} = 1/\sqrt{\ell_{dm}c_{dm}}$. Once the DM current $I_{dm}(z)$ and the DM voltage $V_{dm}(z)$ are known at each line position z , the first-order TL equations for the CM circuit can be re-written as:

$$\frac{dV_{cm}(z)}{dz} + j\omega\ell_{cm}I_{cm}(z) = -j\omega\Delta L I_{dm}(z); \quad \frac{dI_{cm}(z)}{dz} + j\omega c_{cm}V_{cm}(z) = -j\omega\Delta C V_{dm}(z); \quad (34)$$

where the right-hand side contributions act as infinitesimal voltage and current sources, respectively, distributed along the CM line. Integration of these infinitesimal sources along the line length allows representing DM-to-CM conversion by lumped current and voltage sources connected at the right termination of the CM circuit as shown in Figure 5(b). After some cumbersome algebra (not reported here for the sake of brevity), the dependent sources driving the CM circuit can be cast in closed form as:

$$V_{\Delta} = -j\omega [\Delta L Sh_1 + \Delta C Z_{cm} Z_{dm} Sh_2] I_{dm}(0) + j\omega [\Delta L Z_{dm}^{-1} Ch_1 + \Delta C Z_{cm} Ch_2] V_{dm}(0), \quad (35)$$

$$I_{\Delta} = j\omega [\Delta L Z_{cm}^{-1} Ch_2 + \Delta C Z_{dm} Ch_1] I_{dm}(0) - j\omega [\Delta L Z_{cm}^{-1} Z_{dm}^{-1} Sh_2 + \Delta C Sh_1] V_{dm}(0), \quad (36)$$

where:

$$Sh_2 = v_{dm}^{-1} \frac{\sinh(j\omega\ell/v_{dm})}{j\omega(v_{dm}^{-2} - v_{cm}^{-2})} - v_{cm}^{-1} \frac{\sinh(j\omega\ell/v_{cm})}{j\omega(v_{dm}^{-2} - v_{cm}^{-2})}, \quad (37)$$

$$Ch_2 = v_{dm}^{-1} \frac{\cosh(j\omega\ell/v_{dm}) - \cosh(j\omega\ell/v_{cm})}{j\omega(v_{dm}^{-2} - v_{cm}^{-2})}, \quad (38)$$

and $Z_{cm} = \sqrt{\ell_{cm}/c_{cm}}$, $v_{cm} = 1/\sqrt{\ell_{cm}c_{cm}}$ denote the CM characteristic impedance and propagation velocity, respectively.

Conversely, mode conversion due to termination imbalance is not influenced by medium un-homogeneity. Hence, the circuit interpretation in Figure 5(a), as well as the analytical expressions in (20), (21) are still valid.

7.2. Implementation in SPICE

As an explicative example for circuit implementation in SPICE, the 1 m-long DL characterized by the geometrical parameters in Subsection 3.2 and imbalance coefficients in Section 6 (i.e., $\Delta h = d/2$, $\Delta Z_L = \Delta Z_R = 0.05 Z_D/2$) is here re-considered with the two wires surrounded by a dielectric jacket with thickness $t = 0.3$ mm and relative dielectric permittivity $\epsilon_r = 2.5$. For this wiring structure, numerical evaluation [22] of the modal p.u.l. inductance and capacitance parameters in (31)–(32) yields the values: $\ell_{cm} = 894.8$ nH/m, $c_{cm} = 12.88$ pF/m, $\ell_{dm} = 626.6$ nH/m, $c_{dm} = 22.33$ pF/m, $\Delta L = 2.3$ nH/m, $\Delta C = -0.05$ pF/m, hence: $Z_{dm} = 167.5 \Omega$, $Z_{cm} = 263 \Omega$, $v_{dm} = 2.67 \cdot 10^8$ m/s, $v_{cm} = 2.945 \cdot 10^8$ m/s.

The obtained SPICE schematic is shown in Figure 12(a). Likewise in Figure 11(a), separate evaluation of the contributions to the overall CM voltages due to line and termination imbalance is achieved by the use of three two-conductor TLs here implemented by TLOSSY parts with p.u.l. parameters ℓ_{dm} , c_{dm} , ℓ_{cm} , c_{cm} . The loads at the terminations of the DM circuit (TL in the middle) are matched, that is: $Z_D = Z_{dm} = 167.5 \Omega$. The CM circuits (upper and lowest TLs) are terminated by CM impedances $Z_{GL(R)} + Z_D/4 \approx 1$ k Ω .

The contribution due to termination imbalance is predicted by the lowest CM circuit, which is here driven by current-controlled voltage sources with gain $|\Delta Z_L| = \Delta Z_R = 4.188 \Omega$.

As regards line imbalance (upper CM circuit), implementation in SPICE of the voltage and current sources V_{Δ} , I_{Δ} in (35)–(38) is achieved by the use of two ABM parts (e.g., ELAPLACE or GLAPLACE [21]) for each source [instead of only one as in Figure 11(b)]. To this end, (35)–(38) are re-written in terms of Laplace transform as:

$$V_{\Delta}(s) = z_{\Delta}(s) I_{dm}(0) + \alpha_{\Delta}(s) V_{dm}(0), \quad I_{\Delta}(s) = \beta_{\Delta}(s) I_{dm}(0) + y_{\Delta}(s) V_{dm}(0), \quad (39)$$

where $z_{\Delta}(s)$, $y_{\Delta}(s)$, $\alpha_{\Delta}(s)$, $\beta_{\Delta}(s)$ denote the frequency-dependent gains of the involved voltage- and current-controlled voltage and current sources. To ease SPICE implementation, expressions for such gains are further reworked, and cast as function of two numerical coefficients only, i.e.,

$$k_{\Delta,1} = \frac{v_{dm} v_{cm}}{v_{cm}^2 - v_{dm}^2} \left(v_{dm} \frac{\Delta L}{dm} + v_{cm} \frac{\Delta C}{cm} \right), \quad (40)$$

as

$$\begin{aligned} z_{\Delta}(s) &= -k_{\Delta,1} \sinh(s\ell/v_{dm}) + k_{\Delta,2} \sinh(s\ell/v_{cm}), \\ \alpha_{\Delta}(s) &= Z_{dm}^{-1} k_{\Delta,1} [\cosh(s\ell/v_{dm}) - \cosh(s\ell/v_{cm})], \\ \beta_{\Delta}(s) &= Z_{cm}^{-1} k_{\Delta,2} [\cosh(s\ell/v_{dm}) - \cosh(s\ell/v_{cm})], \\ y_{\Delta}(s) &= Z_{cm}^{-1} Z_{dm}^{-1} [k_{\Delta,1} \sinh(s\ell/v_{cm}) - k_{\Delta,2} \sinh(s\ell/v_{dm})], \end{aligned} \quad (41)$$

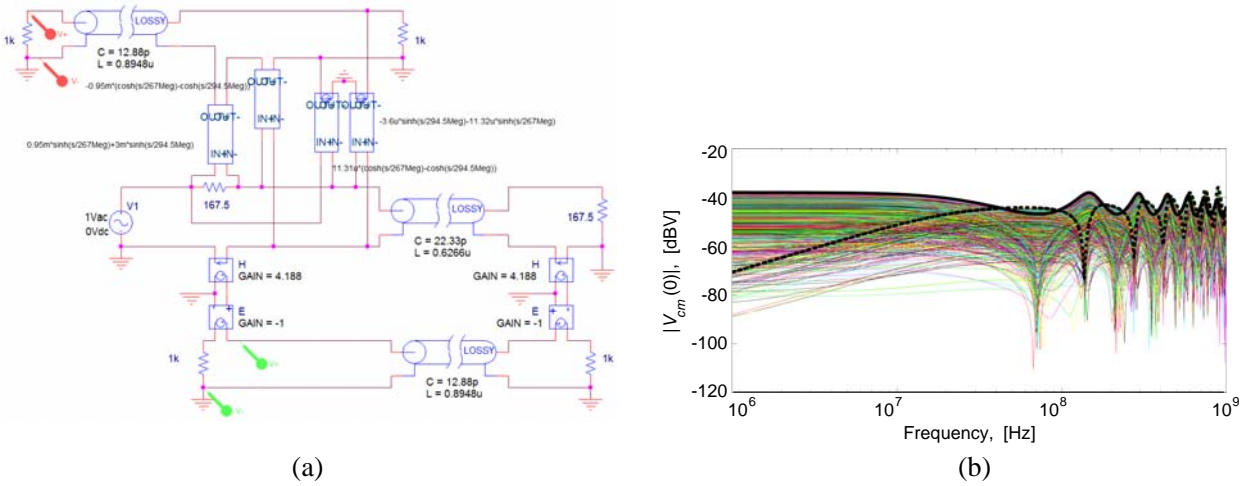


Figure 12. Inhomogeneous medium: (a) SPICE schematic of the unbalanced DL excited by a DM source. (b) SPICE predictions (black curves) vs 1000 repeated simulations obtained by exact solution of MTL equations (left TL end).

which can be assigned as gains of the involved ABM parts more easily than those in (35)–(38). Note that, due to the lack of current-controlled ABM sources, the current-controlled sources in (39) were implemented as voltage-controlled ABM sources dependent on the voltage drop across the series impedance Z_D . Accordingly, the gains of these sources — i.e., coefficients $z_\Delta(s)$, $\beta_\Delta(s)$ — were further divided by $Z_{dm} = 167.5 \Omega$.

7.3. Worst-Case Analysis

Use of the SPICE schematic in Figure 12(a) for worst-case prediction of the CM voltages at DL terminations is here exemplified by assuming imbalance coefficients randomly spread within the intervals: $-d/2 \leq \Delta h \leq d/2$, and $-0.05Z_D/2 \leq \Delta Z_L, \Delta Z_R \leq 0.05Z_D/2$ (as in Section 6.1).

Likewise for the homogeneous case, only two runs of the SPICE schematic can suffice to this purpose. However, since the contribution due to line imbalance [see Eq. (40)] is now depending on an inductive and a capacitive coefficient (ΔL , ΔC , respectively), which are (a) always opposite in sign and (b) not related each other by straightforward relationships (as in the homogeneous case), the two simulations have to be run in either one of the following two sets of conditions. If ΔC is assumed to be positive, one simulation shall be run with $\Delta Z_L > 0$ and $\Delta Z_R > 0$, the other (simulation leading to the flat frequency response at low frequency) with $\Delta Z_L < 0$ and $\Delta Z_R > 0$. Vice versa, if ΔC is assumed to be negative (and, as a consequence, ΔL is positive), one simulation requires $\Delta Z_L < 0$ and $\Delta Z_R < 0$, the other involves $\Delta Z_L > 0$ and $\Delta Z_R < 0$.

Effectiveness of the obtained upper bounds (dashed- and solid-black curves, respectively) is proven in Figure 12(b), by comparison versus 1000 repeated simulations based on exact solution of MTL equations (colored curves) with imbalance coefficients randomly selected within the intervals under analysis.

8. CONCLUSION

Based on the assumption of weak imbalance, a SPICE model has been developed, which allows prediction of modal voltages/currents at the terminations of a DL-circuit affected by undesired imbalance due to asymmetries in the line cross-section (line imbalance) and/or in the terminal networks (termination imbalance). Model accuracy has been validated versus exact solution of MTL equations, and suitable guidelines have been derived and discussed to enable worst-case prediction of the involved modal quantities by a limited number of simulations. The model has been derived in detail for

DM-to-CM conversion, at the basis of REs, and then extended to CM-to-DM conversion, which is responsible for radiated [6] and conducted susceptibility [8]. Duality between the two conversion mechanisms has been verified in the case of ground impedances equal to zero, which corresponds to the measurement conditions foreseen by International Standards for experimental evaluation of Longitudinal and Transverse Conversion Loss parameters (LCL and TCL, respectively) [11, 13].

Although derived for a canonical DL structure, the proposed model can be extended to handle more complex wiring harnesses and terminal networks (e.g., terminal networks characterized at the input pins by measurement can be easily included into the model). Additionally, the proposed modeling approach, based on the representation of the unbalanced line as a perturbation of the corresponding balanced structure, can be efficiently exploited to perform sensitivity analysis of undesired modal quantities to the inherently uncertain and uncontrolled parameters at the basis of mode conversion.

REFERENCES

1. Boni, A., A. Pierazzi, and D. Vecchi, "LVDS I/O interface for Gb/s per pin operation in 0.35- μm CMOS," *IEEE Jour. Solid-State Circuits*, Vol. 36, No. 4, 706–711, 2001.
2. Kami, Y., F. Xiao, and K. Murano, "Mode-port-network approach to analyze power-line EMC problems for PLC," *Proc. 20th Int. Zurich Symp. on Electromagn. Compat.*, 9–12, Zurich, Switzerland, 2009.
3. Haggmann, J. H. and S. Dickmann, "Determination of mode conversion on differential lines," *Proc. EMC Europe 2008*, 1–5, Hamburg, Germany, 2008.
4. Shimazaki, M. and H. Asai, "Evaluation method of balance mismatch using CMRR measurement for printed circuit board," *Proc. Asia-Pacific EMC Conference (APEMC)*, 101–104, Tokyo, Japan, 2014.
5. Kayano, Y., Y. Tsuda, and H. Inoue, "Identifying EM radiation from asymmetrical differential-paired lines with equi-distance routing," *Proc. IEEE Int. Symp. EMC*, 311–316, Pittsburgh, USA, 2012.
6. Grassi, F., G. Spadacini, and S. A. Pignari, "The concept of weak imbalance and its role in the emissions and immunity of differential lines," *IEEE Trans. Electromagn. Compat.*, Vol. 55, No. 6, 1346–1349, 2013.
7. Miri, M. and M. McLain, "Electromagnetic radiation from unbalanced transmission lines," *Progress In Electromagnetics Research B*, Vol. 43, 129–150, 2012.
8. Grassi, F. and S. A. Pignari, "Bulk current injection in twisted-wire pairs with not perfectly balanced terminations," *IEEE Trans. Electromagn. Compat.*, Vol. 55, No. 6, 1293–1301, 2013.
9. Grassi, F. and S. A. Pignari, "Immunity to conducted noise of data transmission along DC power lines involving twisted-wire pairs above ground," *IEEE Trans. Electromagn. Compat.*, Vol. 55, No. 1, 195–207, 2013.
10. Paul, C. R., *Introduction to Electromagnetic Compatibility*, J. Wiley and Sons, New York, 2006.
11. ITU-T Recommendation G.117, "Transmission aspects of unbalance about earth," Switzerland, 1989.
12. Smith, S. B., S. S. Agili, and V. Balasubramanian, "Theory and measurement of unbalanced differential-mode transmission lines," *Proc. DesignCon. 2006*, 2006.
13. Rohde & Schwarz, "Measuring balanced components with vector network analyzer ZVB," App. Note 1EZ53, Sep. 2004.
14. Wu, X., Y. Yang, F. Grassi, G. Spadacini, and S. A. Pignari, "Statistical characterization of line-imbalance in differential lines," *Proc. XXXIth General Assembly of International Union of Radio Science (URSI)*, Beijing, P. R. China, 2014.
15. Grassi, F., Y. Yang, X. Wu, G. Spadacini, and S. A. Pignari, "On mode conversion in geometrically unbalanced differential lines and its analogy with crosstalk," *IEEE Trans. Electromagn. Compat.*, Early Access Article, DOI: 10.1109/TEMC.2014.2372894.

16. Xie, H., J. Wang, R. Fan, and Y. Liu, "Study of loss effect of transmission lines and validity of a spice model in electromagnetic topology," *Progress In Electromagnetics Research*, Vol. 90, 89–103, 2009.
17. Xie, H., J. Wang, R. Fan, and Y. Liu, "SPICE models for radiated and conducted susceptibility analyses of multiconductor shielded cables," *Progress In Electromagnetics Research*, Vol. 103, 241–257, 2010.
18. Caniggia, S. and F. Maradei, "SPICE-like models for the analysis of conducted and radiated immunity of shielded cables," *IEEE Trans. Electromagn. Compat.*, Vol. 46, No. 4, 606–616, 2004.
19. Kung, F. W. L. and H. T. Chuah, "System modeling of high-speed digital printed circuit board using SPICE," *Progress In Electromagnetics Research*, Vol. 20, 179–211, 1998.
20. Shi, X., W. M. Lim, M. A. Do, and C. C. Boon, "A SPICE compatible model of on-wafer coupled interconnects for CMOS RFICS," *Progress In Electromagnetics Research*, Vol. 102, 287–299, 2010.
21. Cadence-Orcad, *PSPICE User Guide*, 2000.
22. Clements, J. C., C. R. Paul, and A. T. Adams, "Computation of the capacitance matrix for systems of dielectric-coated cylindrical conductors," *IEEE Trans. Electromagn. Compat.*, Vol. 17, No. 4, 238–248, 1975.